DEVELOPMENTAL BIOLOGY 136, 430-445 (1989)

Local Shifts in Position and Polarized Motility Drive Cell Rearrangement during Sea Urchin Gastrulation

JEFF HARDIN

Department of Zoology, Duke University, Durham, North Carolina 27706

Accepted August 10, 1989

This study examines the mechanisms of epithelial cell rearrangement during archenteron elongation in the sea urchin embryo using scanning electron microscopy, differential interference contrast videomicroscopy, cell marking, and fluorescently labeled chimaeric clones. Archenteron elongation involves two major processes: *local shifts in position* of cells in the archenteron wall and *polarized motility* of the cells as they rearrange. Fluorescently labeled chimaeric clones introduced into the archenteron of *Lytechinus pictus* are initially 4-5 cells wide; by the end of gastrulation the clones elongate and narrow, so that they are one cell wide in the narrowest region of the archenteron. The extent of clonal mixing indicates that cells in the archenteron change their relative positions by only 1-2 cell diameters during cell rearrangement. Cells at the blastopore rearrange concomitantly with cells in the archenteron, resulting in a 35% decrease in blastopore diameter. Endoderm cells undergo polarized, stage-specific changes in shape and motility as they rearrange: (1) they flatten markedly along their apical-basal axis throughout archenteron elongation; (2) just prior to the onset of cell rearrangement, basal surfaces of all cells in the archenteron extend long, polarized lamellipodial protrusions along the axis of extension of the archenteron; (3) as cell rearrangement begins, basal surfaces round up and the cells become isodiametric; (4) by the $\frac{3}{4}$ gastrula stage the cells become stretched along the animal-vegetal axis, apparently due to filopodial traction, and finally (5) they continue to rearrange, returning to a less elongated shape by the end of gastrulation. Direct observation of gastrulation in the cidaroid *Eucidaris tribuloides* indicates that in this species cell rearrangement is accomplished by progressive circumferential intercalation of cells without upwardly directed filopodia. This intercalation is accompanied by explosive, apparently stochastic, cortical blebbing activity at the boundaries between cells, suggesting that in addition to whatever cell rearrangement may be generated by filopodial tension, such activity is an important component of the active rearrangement process.

INTRODUCTION

How are sheets of cells remodeled as the shape of the embryo is transformed during gastrulation? The sea urchin embryo has served as a paradigm for answering this question since the beginnings of experimental embryology. One of the most striking events that occurs during gastrulation in the sea urchin embryo is the inward bending of the vegetal plate to form the archenteron. The invagination of the archenteron occurs in two stages: (1) primary invagination, during which the vegetal plate bends inward to form a short, stout archenteron and (2) secondary invagination, during which the archenteron elongates across the blastocoel (Gustafson and Kinnander, 1956). Recently it has been shown that the epithelial cells of the archenteron rearrange as it elongates (Ettensohn, 1985; Hardin and Cheng, 1986). Much of this rearrangement occurs without filopodial traction by secondary mesenchyme cells, since it takes place in both LiCl-induced exogastrulae (Hardin and Cheng, 1986), and in embryos in which secondary mesenchyme cells have been ablated with a laser microbeam (Hardin, 1988). Thus archenteron elongation must presumably involve active rearrangement of epithelial cells independent of traction exerted by the filopodia.

Although the phenomenon of epithelial cell rearrangement in the archenteron has been well established, virtually nothing is known about the motile behavior that produces it. The time-lapse ciné filming (Gustafson and Kinnander, 1956; Kinnander and Gustafson, 1960) and videomicrography (Hardin, 1988) performed to date have suggested that little obvious protrusive activity occurs in the wall of the archenteron as it elongates. A preliminary investigation of the early stages of gastrulation in *Lytechinus pictus* using scanning electron microscopy has noted that just prior to secondary invagination, the basal surfaces of cells in the archenteron wall extend lamellipodial protrusions along the animal-vegetal axis (Ettensohn, 1984b); however, the importance and detailed character of these protrusions have not been studied. At the cytoskeletal level, the rearrangement process does not appear to require intact cytoplasmic microtubules (Hardin, 1987), but little information is available regarding the presumably actin-mediated motility that generates rear-

0012-1606/89 $3.00

rangement. In addition, it is not known how local patterns of cell rearrangement in the archenteron are coordinated globally to produce its extension.

In order to address these questions, this study uses scanning electron microscopy, time-lapse videomicrography, cell marking, and fluorescently labeled chimaeric clones to investigate stage-specific changes in protrusive activity, cell shape, and cell position that occur as cells rearrange in the archenteron of the sea urchin embryo. The results indicate that secondary invagination in the euechinoid, *L. pictus*, involves very local cell rearrangements accompanied by coordinated, polarized changes in cell motility and cell shape. These cell rearrangements simultaneously elongate the archenteron and close the blastopore. In addition, direct observations of cell rearrangement in the archenteron have been made for the first time by exploiting the superb optical properties of the cidaroid urchin, *Eucidaris tribuloides*. These observations indicate that a major mechanism of cell rearrangement in this species is the progressive circumferential intercalation of epithelial cells in the wall of the archenteron, accompanied by explosive cortical blebbing activity on the part of the rearranging cells. Some of these results have appeared previously in abstract form (Hardin, 1986).

MATERIALS AND METHODS

Procurement of embryos. Gametes of *L. pictus* (Marinus) and *E. tribuloides* (Carolina Biological) were obtained, fertilized, and cultured at 16°C (*L. pictus*) or 19–22°C (*E. tribuloides*) as described previously (Hardin and Cheng, 1986).

Tissue sectioning and videomicroscopy. Embryos were fixed in 0.75% glutaraldehyde in 90% MFSW for 1 hr at 16°C and postfixed in 1% OsO_4 in MFSW buffered with 0.05 *M* sodium cacodylate, pH 8.0, for 1 hr at 4°C in the dark. Postfixed embryos were dehydrated in ethanol and embedded in Spurr's resin. Sections were cut at 1–2 μm and stained with either toluidene blue with 1% sodium borate or methylene blue/azure II. Time-lapse videomicroscopy of embryos was performed as described in Hardin and Cheng (1986). To analyze cell rearrangements during gastrulation in *E. tribuloides*, tracings of the video monitor were made onto acetate, and the resulting cell outlines were retraced using the morphometrics procedures outlined below.

Vital dye marking. Micropipets pulled from Omega dot glass capillary tubing (0.75 mm i.d., 1.0 mm o.d; Frederick Haer and Co., Brunswick, ME) on a Narishige horizontal puller were manually broken with fine forceps to yield a tip with i.d. ~2 μm. Early *L. pictus* gastrulae in MFSW were attached to a poly-L-lysine-coated tissue culture dish, and eight embryos were marked by repeated extrusion of a freshly filtered solution of 1% Nile blue sulfate (Sigma) in distilled water from a micropipet placed snugly against the surface of the embryo. Over the time period of interest, the dye remained localized to the point of application.

Fluorescent chimaeras. L. pictus chimaeras were produced using the procedures of Wray and McClay (1988), except that donor embryos were dissociated at the 16-cell stage by settling twice through ice-cold hyaline extraction medium (McClay, 1986), resuspending in cold calcium-free artificial sea water (CF-ASW), and gently triturating with a long-bore Pasteur pipet. After collection of the labeled macromere-enriched fraction, host embryos and donor cells were combined in finger bowls, allowed to settle for 20 min, and were then rinsed with ASW. At the blastula stage embryos were transferred to stirring cultures until the gastrula stage.

Volume and blastopore measurements. Blastopore measurements were made from living *L. pictus* embryos photographed through the midsagittal optical plane of section. Volume measurements were made from 1-μm plastic sections by calculating the volume of the solid of revolution obtained by rotating small slices of the section about the animal-vegetal axis. This method is accurate when compared to volume measurements made from serial reconstructions of sectioned specimens (Ettensohn, 1984a).

Scanning electron microscopy. For examining outer surfaces of the archenteron, embryos were fixed in 1–2.5% glutaraldehyde, postfixed, dehydrated, and critical-point dried from CO_2. Dried embryos were transferred to double-sided adhesive tape (Scotch brand; 3M Co.) attached to aluminum stubs, and fractured under a stereomicroscope using glass needles mounted in a Leitz joystick micromanipulator. For fracturing archenterons, embryos were fixed according to Amemiya *et al.* (1983) in 2% OsO_4 in a sucrose-cacodylate buffer containing 0.6 *M* sucrose and 0.1 *M* sodium cacodylate in distilled water, pH 6.4, and processed as above. Fractured embryos were coated with gold-palladium and viewed using an ISI-DS 130 or JEOL T20 scanning electron microscope. Cell counts performed on specimens processed for SEM were obtained by counting all visible cells in the front-facing half of the archenteron, and multiplying this value by two.

Morphometrics. Morphometrics were performed using either a system described previously (Hardin and Keller, 1988), or a Summagraphics MacTablet connected to a Macintosh II computer and *MacMorph*, a morphometrics program written by the author and based on *MacMeasure*, a public domain morphometrics program (Hook and Rasband, 1987). Two important parameters derived from these programs are the LW ratio and the YX ratio. The LW ratio provides a measure of

the elongation of a cell along its own long axis, while the YX ratio is a measure of the elongation of a cell in a specified direction (Hardin and Keller, 1988). For measurements of cells in the wall of the archenteron, the relevant external direction for YX ratio measurements was the long axis of the archenteron (i.e., the animal-vegetal axis); for measurements at the blastopore, the YX ratio represents the length of a cell in the radial direction divided by its width in the circumferential direction. For morphometric measurements, stages of gastrulation in *Eucidaris* are defined as follows: early, cylindrical archenteron that has reached ~20% of its final length, with few or no detectable filopodia; mid, active filopodia, 40–60% extension; late, loose mesenchyme at the tip of the archenteron, 80–100% extension. Near-neighbor analysis was performed by counting the number of immediately adjoining cells surrounding a given cell in the archenteron from SEM micrographs. Shortest unbiased confidence limits for near-neighbor variances were determined according to Sokal and Rohlf (1981); statistical comparisons using ANOVA and the Student-Newman-Keuls multiple comparison test were carried out according to Zar (1984). Autocorrelation analyses were performed using *Statgraphics* statistical software (STSC, Inc.).

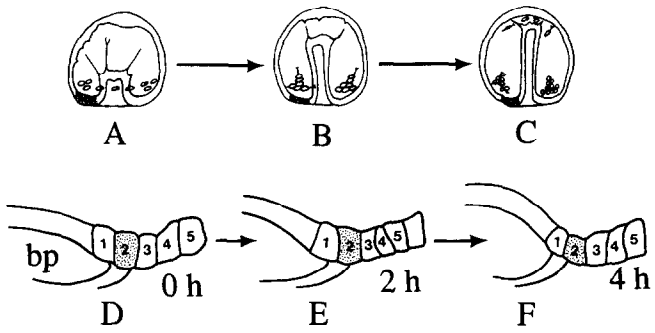

FIG. 1. Measurements of involution during secondary invagination in *L. pictus*. (A–C). Application of a spot of Nile blue sulfate at the blastopore lip prior to the onset of secondary invagination. The spot does not translocate during secondary invagination. (D–F) Movements at the blastopore lip studied using time-lapse videomicroscopy. The same group of cells (labeled 1–5) was followed during secondary invagination (approximately 4 hr in duration at 23°C); the cells do not translocate into the invaginating region. bp, blastopore.

RESULTS

No Cells Are Added to the Archenteron during Secondary Invagination in L. pictus

The total number of cells in the archenteron does not change during secondary invagination in *L. pictus*, on the basis of cell counts made from scanning electron micrographs. The average number of cells in the archenteron at the onset of secondary invagination is 107.3 ± 1.8 (mean ± SEM; $n = 3$), 110.5 ± 1.0 at the $\frac{2}{3}$ gastrula stage ($n = 4$), and 113.4 ± 2.3 at the end of gastrulation ($n = 5$), which is not a significant change at the 95% confidence level ($P = 0.14$). Furthermore, the extent of involution that occurs during secondary invagination appears to be minimal, based on two lines of evidence. When the blastopore lip is stained with a spot of Nile blue at the end of primary invagination, the spot does not translocate over the lip of the blastopore during secondary invagination (Figs. 1A–1C). This is confirmed by time-lapse videomicroscopy. Figures 1D–1F represent successive video records of one of three such experiments. Cells at the blastopore lip observed throughout secondary invagination remain essentially stationary, indicating that little or no involution occurs during secondary invagination in *L. pictus*. Finally, measurements of cellular volume indicate that there is no statistically significant increase in the amount of cellular material in the archenteron during secondary invagination (correlation coefficient, r, not significantly different from 0 at the 95% confidence level). The pooled mean cellular volume is $5.2 \pm 0.1 \times 10^4$ μm^3 (mean ± SEM; $n = 15$) throughout secondary invagination.

Blastopore Closure Occurs via Cell Rearrangement

A plot of blastopore diameter vs archenteron length for *L. pictus* gastrulae at various stages of invagination clearly shows that blastopore closure occurs in two phases (Fig. 2). During primary invagination blastopore closure occurs at a rate greater (with respect to the extent of invagination) than during secondary invagination (as indicated by regression lines with two different slopes in Fig. 2). Furthermore, the behavior of cells at the blastopore lip is distinctly different during primary and secondary invagination. During primary invagination, cells with constricted apices are prominent in the central, invaginated region of the vegetal plate (Fig. 3A). However, at the incipient blastopore lip cell apices are expanded, and the cells appear to be sheared towards the center of the vegetal plate (Fig. 3A). Such behavior may reflect predominantly apical tension exerted by the central, constricted cells, and may also be indicative of translocation of cells into the invagination as it deepens, since it is known that some cells are recruited into the archenteron from its periphery during primary invagination in *L. pictus* (Ettensohn, 1984a).

The situation during secondary invagination is quite different. The blastopore decreases in diameter by ~35% during this time, and this decrease is closely correlated with archenteron length ($-0.51 \leq r \leq -0.98$;

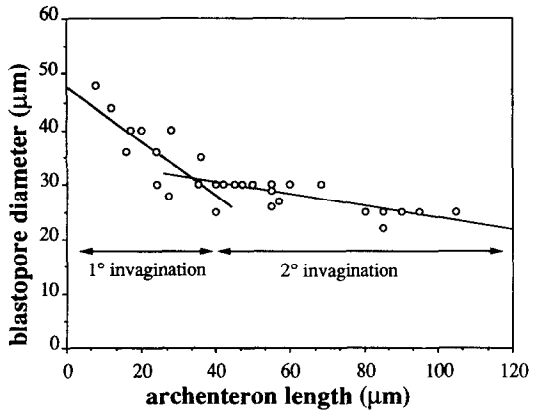

FIG. 2. The relationship between blastopore closure and archenteron length in *L. pictus*. Blastopore diameter was plotted against archenteron length for various stages of invagination. The rate of blastopore closure (with respect to archenteron length) is considerably greater during primary invagination than during secondary invagination.

Fig. 2). Scanning electron microscopy reveals that blastopore closure occurs by rearrangement of cells at the blastopore lip. At the end of primary invagination there are 28–30 cells in a ring around the blastopore and 20–24 cells around the circumference of the archenteron at its base (Fig. 3B). The blastopore continues to decrease in diameter until gastrulation ends; the number of cells around the blastopore declines to 16–18 and is matched by a further drop in the number of cells around the circumference of the archenteron to 10–12 (Fig. 3C). In contrast to the complicated morphologies seen during primary invagination, the apices of cells at the blastopore remain isodiametric during secondary invagination ($\frac{1}{2}$ gastrulae: YX ratio = 0.97 ± 0.15; surface area/cell = 37.1 ± 9.7 μm^2; apical perimeter/cell = 25.1 ± 2.9 μm, mean ± S.D., n = 45 cells; late gastrulae: YX ratio = 1.02 ± 0.20; surface area/cell = 37.3 ± 8.6 μm^2; apical perimeter/cell = 24.4 ± 3.1 μm, n = 43 cells; none are significantly different at the 95% confidence level). Similar results were obtained for *E. tribuloides* (data not shown).

Cells Undergo Local Shifts in Position during Archenteron Elongation in L. pictus

Changes in position of labeled endodermal clones. Several workers have presented evidence that clones of labeled cells within the archenteron change shape as it elongates. The line drawings of Hörstadius (Hörstadius, 1935, Fig. 1A, p. 42) appear to indicate that clones derived from single vitally stained veg_2 blastomeres initially comprise a wedge-shaped patch within the archenteron which is resolved into a thin strip of labeled material by the end of gastrulation. Similarly, Cameron *et al.* (1987) and Wray (1987) have noted that the borders of labeled clones of cells introduced into the archenteron are somewhat jagged, which is suggestive of rearrangement. The present study uses the chimaera technique of Wray (1987) and Wray and McClay (1988) to examine systematically the changes in shape and position of subsets of cells within the archenteron of *L. pictus* as it elongates. Figure 4 shows that labeled clones, descended from either half macromeres or veg_2 cells, initially comprise a contiguous patch within the vegetal plate (Fig. 4A); descendents of half macromeres also contain labeled cells in the presumptive anal ectoderm (Fig. 4C), consistent with their fate in the normal embryo (reviewed by Hörstadius, 1973). Little distortion of clones occurs during primary invagination (Fig. 4A, 4C); the clones are rectangular and 4–5 cells-wide at the end of primary invagination. During secondary invagination, however, labeled clones change shape dramatically. By the end of gastrulation the clone is often only one cell wide in the thinnest region of the gut rudiment; the width of the clone gradually increases toward the base and tip regions, where the clone remains 2–3 cells-wide (Fig. 4E). In embryos in which incomplete incorporation of the clone has occurred, or in which a smaller descendent blastomere has generated the clone, the clone may actually be discontinuous, with one or two neighboring, unlabeled cells intercalated between cells of the clone (Fig. 4G). However, in all cases the rearrangement of clonal boundaries does not appear to involve shifts of cell position of more than two cell diameters.

Departures from hexagonal packing during cell rearrangement. It has been argued that the geometric constraints imposed on rearranging epithelia should force departures from the hexagonal cell packing pattern found in most epithelia (i.e., six near-neighbors surrounding a given cell; Fristrom, 1976). Table 1 compares the mean number of near-neighbors and associated variance for cells in the archenteron at various stages of secondary invagination. The mean number of near-neighbors at all stages is very nearly six, but the variances differ markedly. In particular, although deviations from hexagonal packing are fairly infrequent at the $\frac{1}{2}$ gastrula stage, departures from hexagonal packing are common at the $\frac{2}{3}$ gastrula stage. Fewer deviations occur during subsequent stages, although the regularity of cell packing never fully returns to the level prior to extensive cell rearrangement (Table 1).

Changes in Cell Shape and Protrusive Activity in the Archenteron of L. pictus: Initial Polarization of Cells Followed by Transient Stretching

Endoderm cells are initially polarized along the axis of extension. Striking, stage-specific changes in the shape

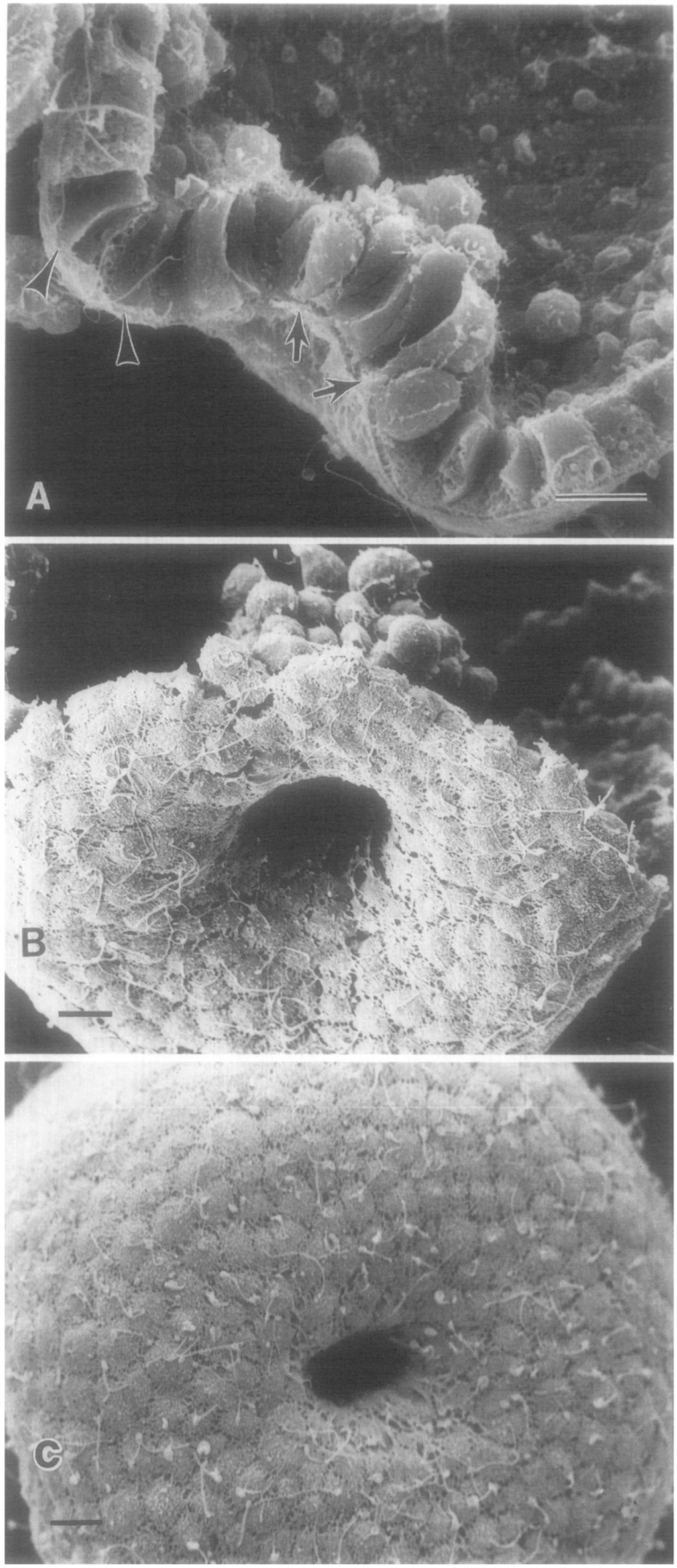
A
B
C

and protrusive activity of the basal surfaces of cells in the wall of the archenteron occur as its cells rearrange. Prior to the onset of secondary invagination, the basal surfaces of endoderm cells are rounded (Fig. 5A). As initially described by Ettensohn (1984b) and confirmed in more detail here, just prior to cell rearrangement the basal surfaces of the cells in the wall of the gut rudiment undergo a dramatic change not visible in the light microscope: long, highly oriented lamellipodial protrusions are extended by each cell toward the animal pole (Fig. 5B). These sheet-like protrusions are 0.5–1.0 μm in thickness, 5–10 μm in length along the animal-vegetal axis, and 2–3 μm in width at their bases. The lamellipodia overlap one another, giving the archenteron a "shingled" appearance. They end in shorter, filopodial protrusions that extend onto the basal surfaces of cells in overlying tiers, generally at an angle to the long axis of the archenteron. Transverse fractures reveal that the cell body and apex do not undergo a corresponding elongation, and thus the cells are L-shaped in profile, with the cell body extending radially outward from the lumen of the archenteron (Fig. 5C). The axis of extension of these lamellipodia does not correspond to the intrinsic apical-basal polarity of the epithelium, but is instead roughly perpendicular to it. This change in the basal morphology of cells in the archenteron also occurs in *Strongylocentrotus purpuratus* and *Lytechinus variegatus* (data not shown).

As cell rearrangement begins, the oriented protrusions disappear; the basal surfaces of the cells become rounded, and a dense, overlapping network of slender protrusions is visible between cells (Fig. 5D). Stereo SEM indicates that some of these protrusions extend into the clefts between the basal surfaces of neighboring cells. Many of these protrusions are not taut, but instead appear loosely curled (Fig. 5D, arrows). At the ½ gastrula stage, these filopodial protrusions disappear, and are replaced by small, filiform protrusions which are ~0.5 μm in length and ~0.1 μm in diameter. Basal surfaces of the endoderm cells appear rounded and smooth at this stage, and are not elongated appreciably along the axis of extension of the archenteron (Fig. 6A; LW ratio = 1.32 ± 0.03, YX ratio = 1.18 ± 0.04; mean ± SEM, n = 60 cells).

Endoderm cells are transiently stretched late in gastrulation. By the ⅔ gastrula stage, the cells of the archenteron wall begin to elongate along the animal-vegetal axis; the mean LW ratio rises to 1.45 ± 0.05, and the YX ratio increases to 1.29 ± 0.05 (n = 45 cells). Elongation of the cells continues through the ¾ gastrula stage; the LW ratio reaches 1.75 ± 0.05, and the YX ratio rises to 1.59 ± 0.05 (n = 75 cells). By the end of gastrulation, further cell rearrangement has occurred in the narrowest region of the archenteron. The cells decrease their radial thickness markedly, and the outer surface of the archenteron becomes covered with an increasingly thick layer of extracellular matrix material. The cells of the gut rudiment are not as elongated on average as during the preceding stage; the preferential elongation of the basal surfaces along the animal-vegetal axis largely disappears (YX ratio = 1.24 ± 0.05, n = 45 cells), although individual cells retain some residual, unoriented, basal elongation (LW ratio = 1.39 ± 0.05). However, this elongation probably does not accurately reflect the "averaged" elongation of a given cell throughout its thickness, since the basal surfaces possess thin extensions on their vegetal and animal margins that contribute significantly to the apparent basal length of the cell. Occasionally cells show extreme elongation in the animal-vegetal direction, such that their YX ratio may be as high as three. These cells are invariably located in the narrowest region of the archenteron; several such cells are almost always found together, giving the strong impression that they are under considerable tension (Fig. 6B). Such stretching also occurs in *S. purpuratus* and *L. variegatus* (data not shown).

Basal surfaces undergo two cycles of oriented elongation/relaxation. The changes in cell shape mentioned thus far are stage-specific, and quantifiably different (ANOVA, $P < 10^{-6}$; Fig. 7A). Basal surfaces undergo two cycles of elongation followed by "relaxation" to a more isodiametric shape. The first cycle begins at the onset of secondary invagination with the extension of the polarized lamellipodia, followed by the initiation of cell rearrangement and a reversion to a rounded morphology. The second cycle, accompanied by further cell rearrangement, begins at the ⅔ gastrula stage and peaks at the ¾ gastrula stage, followed by resumption of a less elongated shape by the end of gastrulation.

Cells in the archenteron flatten along the apical-basal axis. The archenteron undergoes two dramatic changes during secondary invagination; in addition to the rearrangement of its cells, the walls of the archenteron thin

FIG. 3. SEM analysis of the blastopore region during secondary invagination in *L. pictus*. (A) Sagittal view of a gastrula during primary invagination. Note the constricted apices in the center of the vegetal plate (arrows) and the apparent shearing of more peripheral cells toward the center of the plate (arrow heads). (B) Surface view of the blastopore at the ½ gastrula stage. Approximately 30 cells ring the blastopore. (C) Surface view of the blastopore at the ¾ gastrula stage. Approximately 18 cells ring the blastopore. Note the smaller diameter of the blastopore compared to (B). Cell apices remain isodiametric. Scale bars = 10 μm.

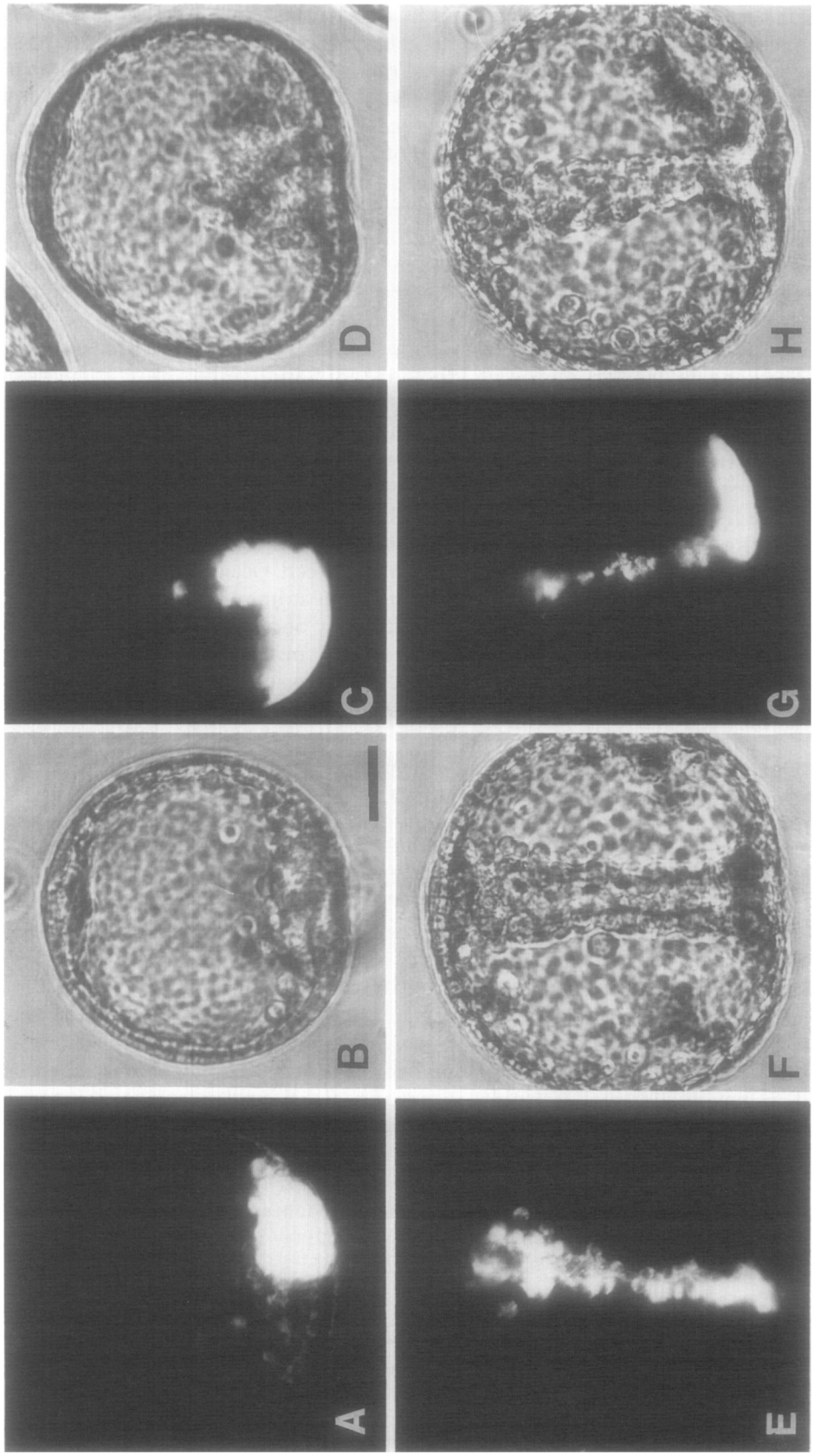

FIG. 4. Deformation of fluorescently labeled chimaeric clones during secondary invagination in *L. pictus*. (A) Rhodamine isothiocyanate-labeled clone in the vegetal plate of an early gastrula. (B) Same embryo as A, bright field. (C) A $\frac{1}{2}$ macromere-derived clone in an embryo at the onset of secondary invagination. The rectangular patch labels both anal ectoderm and endoderm. (D) Same embryo as C, bright field. (E) A veg_2 clone in a late gastrula. The clone is only 1–2 cells wide in the narrowest region of the archenteron. (F) Same embryo as E, bright field. (G) Incorporation of a smaller clone into the archenteron. The clone is discontinuous, with intercalation of 1–2 unlabeled cells between clonally related cells. (G) Same embryo as G, bright field. Scale bar = 20 μm.

TABLE 1
MEAN NUMBER OF NEAR-NEIGHBORS OF CELLS IN THE ARCHENTERON AT VARIOUS STAGES OF SECONDARY INVAGINATION

Stage of elongation	Mean no. near-neighbors[a] (n)[b]	Variance (95% confidence limits)[c]
1/2	5.8 (73)	0.36 ($0.26 < \sigma^2 < 0.51$)
2/3	5.9 (44)	0.94[d] ($0.62 < \sigma^2 < 1.51$)
3/4	5.8 (55)	0.63[d] ($0.44 < \sigma^2 < 0.96$)
Complete	5.8 (54)	0.68[d] ($0.47 < \sigma^2 < 1.04$)

[a] Not significantly different (ANOVA, $P = 0.9$).
[b] Number of cells measured.
[c] Shortest unbiased confidence limits (Sokal and Rohlf, 1981).
[d] Significantly different from 1/2 gastrula stage (Student-Newman-Keuls Test, $P \leq 0.05$; Zar, 1984).

markedly (Dan and Okazaki, 1956; Ettensohn, 1985; Hardin and Cheng, 1986). But how important is the contribution made by cell flattening to archenteron extension? The inner and outer surface area of the archenteron as a whole increase roughly twofold as the archenteron elongates, thereby doubling the total surface area of contact between cells in the archenteron and the basal (blastocoelic) and apical (luminal) extracellular matrix layers by the end of gastrulation. This increase in surface area clearly comes at the expense of lateral contact between cells in the wall of the archenteron ($-0.97 \leq r \leq -0.74$ for wall thickness; $0.77 \leq r \leq 0.97$ for basal surface area/cell; Fig. 7B). The result is an ~40% increase in the circumferential and axial dimensions of the cells, which contributes significantly to the elongation of the archenteron.

Cell Rearrangement Can Be Directly Observed in Eucidaris tribuloides

Cells rearrange by progressive circumferential intercalation. Figure 8 shows differential interference contrast (DIC) videomicrographs of gastrulae of the cidaroid urchin, *E. tribuloides.* The optical clarity and rather loose organization of cells in the archenteron of this species make it possible to observe cell rearrangement events directly using DIC videomicroscopy. In addition, gastrulation in *Eucidaris* is remarkable for another reason. In euechinoids such as *L. pictus*, the filopodia of secondary mesenchyme cells generally point toward the animal pole late in gastrulation (Hardin *et al.*, 1988; Hardin, Morrill and McClay, in preparation). Thus if the filopodia are exerting tension on the archenteron, they would be expected to do so most strongly late in gastrulation. However, in *Eucidaris* the filopodia are few in number well into gastrulation (Schroeder, 1981), and additionally they *never* acquire an appreciably upward orientation (Fig. 8B). Indeed, during much of archenteron elongation many filopodia actually extend *downward* (i.e., vegetally). As laterally directed filopodia exert tension, they can often visibly stretch neighboring endoderm cells; when an individual filopodium retracts, this local deformation ceases. Because filopodia in *Eucidaris* exert sufficient tension to deform the cells of the archenteron, but do not acquire an upward orientation, gastrulation in *Eucidaris* provides a "natural experiment" by which to examine the relative mechanical importance of filopodia to archenteron elongation.

DIC videomicroscopy confirms that cell rearrangement occurs in *Eucidaris* as it does in euechinoids, and provides the first direct observations of cell rearrangement in the archenteron. Tracings of a representative embryo at approximately 30-min intervals are shown in Fig. 8C. The basal surfaces of eight cells have been indicated. At the start of the period of observation, the array of cells is three cell diameters wide and three cell diameters high. Over the next 2 hr, the array of cells gradually narrows and lengthens, so that it comprises an array two cell diameters wide, but five to six cell diameters high. To accomplish this change in the shape of the tissue, the cells must change their position with respect to one another. For example, cells 1 and 5 are initially in contact, but as gastrulation proceeds cells 2 and 3 gradually converge toward one another, with the result that cells 1 and 5 become separated (cf. 0 min with 49 min). A similar intercalation event occurs in the adjacent tier of cells, as cells 6 and 8 converge, resulting in the separation of cells 4 and 7. The other cells in the archenteron are undergoing similar intercalation events, with the result that the entire archenteron elongates by roughly 50% over the period of observation (cf. 0 min with 106 min). The increase in length of the archenteron corresponds very closely to the extent of rearrangement that has occurred; in the example in Fig. 8C the cellular width of the array has narrowed with a concomitant increase in its length that corresponds well to the overall 50% increase in length of the archenteron. As cells intercalate between one another, they generally become elongated circumferentially, so that they are actually wider than they are tall. For example, prior to its intercalation between cells 4 and 7, cell 6 is nearly isodiametric, but as it insinuates itself between its neighbors it becomes elongated (Fig. 8C). Indeed, as gastrulation proceeds in *Eucidaris* the cells of the archenteron as a whole become more elongated in a direction *perpendicular* to its axis of extension, in marked contrast to the situation in *L. pictus* (YX ratios: early, 0.91 ± 0.15, $n = 39$ cells; mid, 0.77 ± 0.18, $n = 43$; late, 0.68 ± 0.20, $n = 41$; significantly different by ANOVA, $P < 0.0001$).

Explosive cortical protrusive activity accompanies cell rearrangement. As the cells of the archenteron rear-

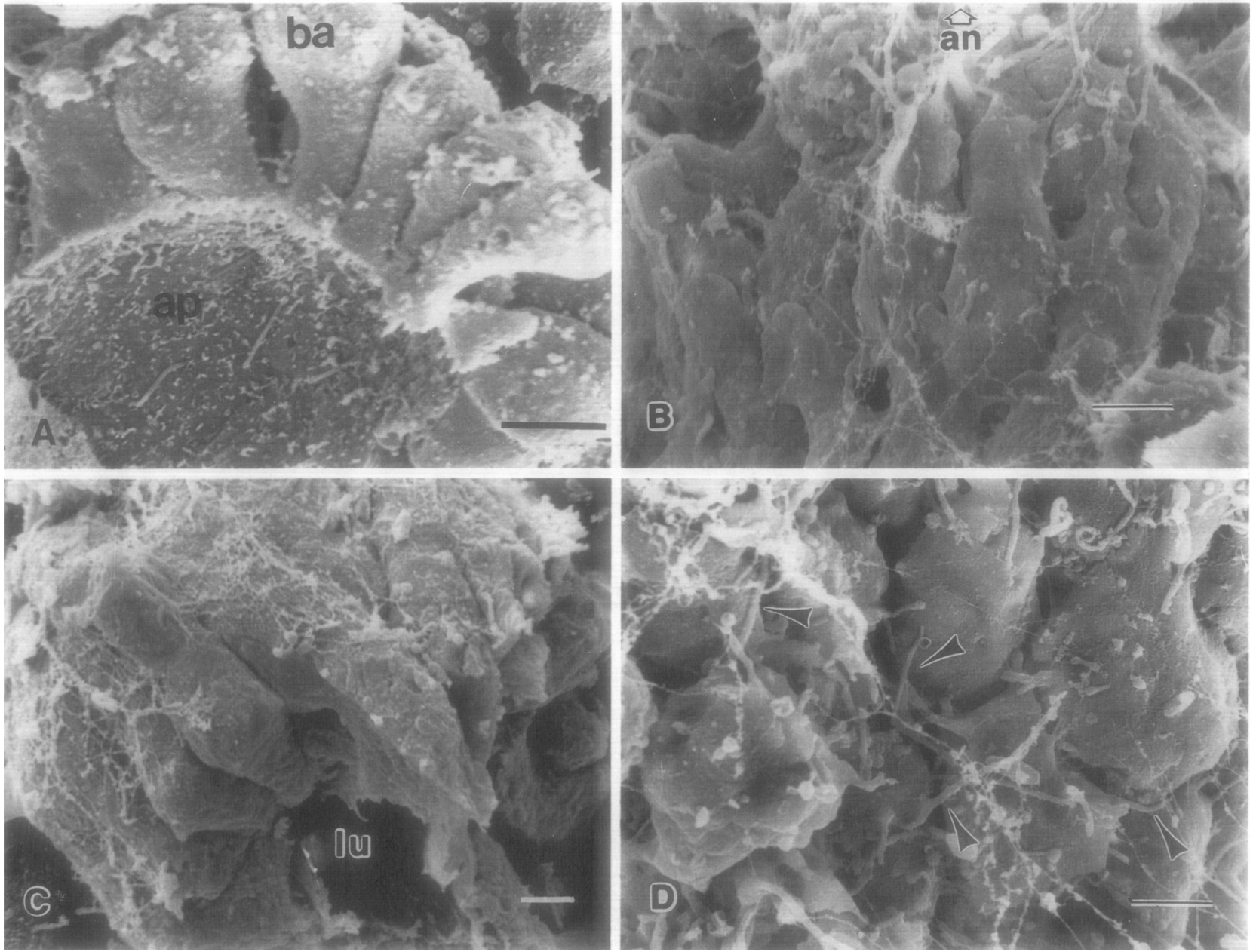

FIG. 5. Changes in protrusive activity at the onset of archenteron elongation. (A) Cellular morphology during primary invagination in *L. pictus*. The hyaline layer/apical lamina has been peeled back to reveal the underlying apical cell surfaces. Note the bulbous basal ends (ba) and the apices studded with microvilli (ap). Bar = 5 μm. (B) Long, oriented basal lamellipodia extend toward the animal pole (an) in the archenteron of a *L. pictus* gastrula at the onset of secondary invagination. Bar = 5 μm. (C) Transverse fracture through an archenteron at the onset of elongation. The cells are L-shaped. lu, lumen of the archenteron. Bar = 2.5 μm. (D) After the lamellipodia recede, basal surfaces display a dense network of filopodia (arrow heads). Note the loose appearance of the protrusions (arrow). Bar = 2.5 μm.

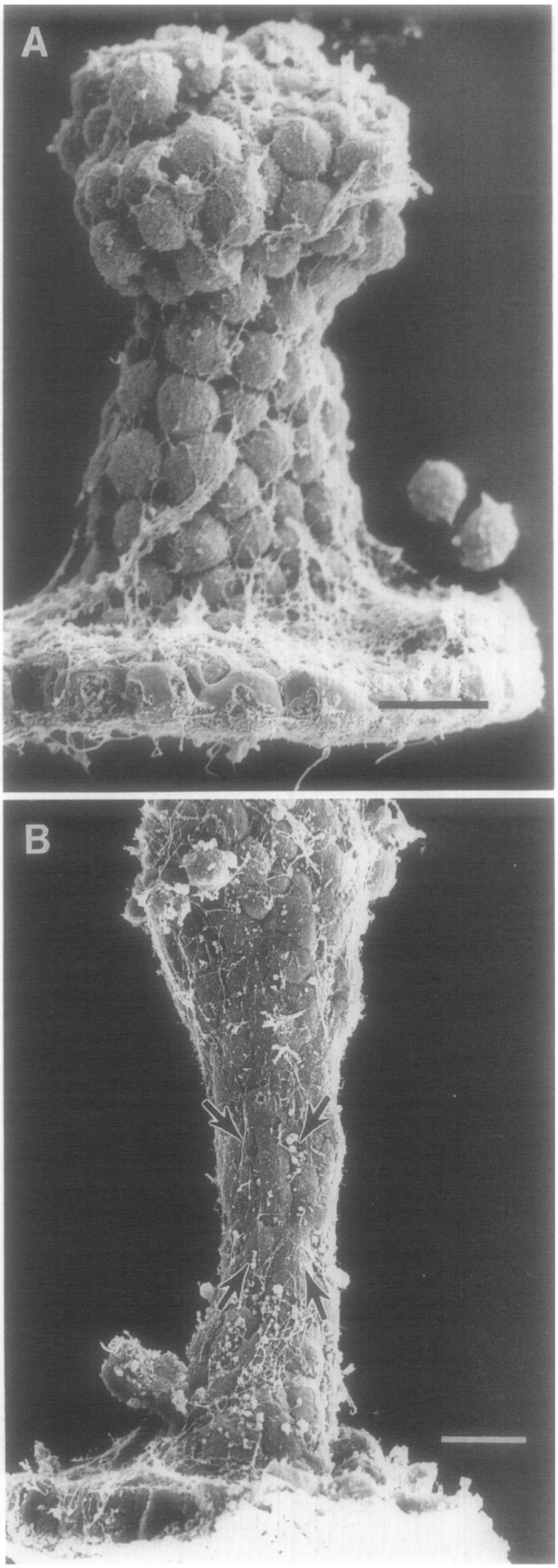

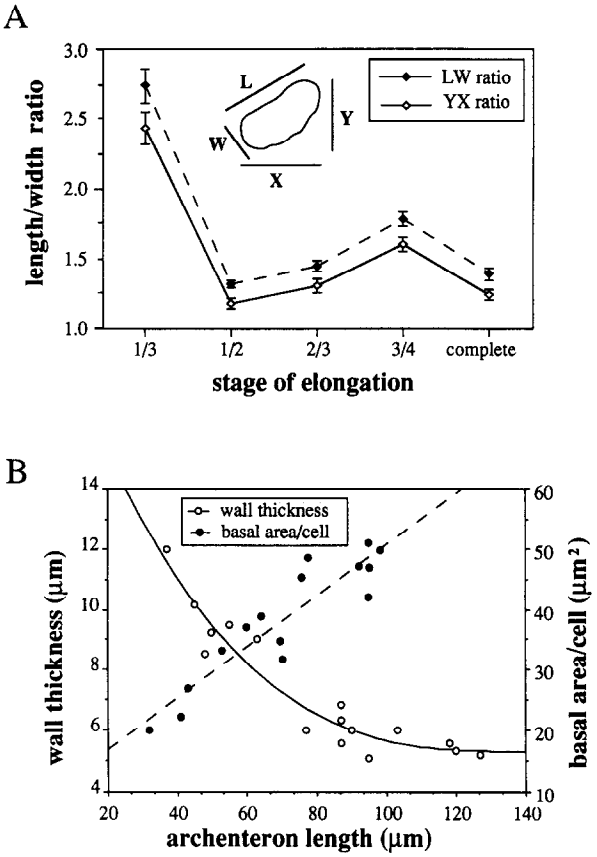

FIG. 7. Changes in the shape of cells in the archenteron as it elongates. (A) Changes in length/width ratios (mean ± SEM) of basal cell surfaces during archenteron elongation in *L. pictus*. The length/width ratio (LW) represents the length of a cell along its own long axis divided by the width along the perpendicular to the long axis. The YX ratio (YX) represents the length of a cell along a specified axis divided by the width in the perpendicular direction (see Materials and Methods for a further description). The reference direction for YX measurements is the long axis of the archenteron. (B) Changes in wall thickness (μm) and basal surface area per cell (μm²) for cells in the archenteron vs archenteron length (μm).

range, they undergo vigorous motile activity. Cortical bleb-like protrusions are continually sent out, they rotate part of the way around the basal periphery of the cell, and then disappear. Tracings of a typical cell made at 20-sec intervals are shown in Fig. 9A. The basal surface extends blebs that have a lifetime of approximately 30 sec (arrows, Fig. 9A). These blebs can traverse as much as 180° as they rotate, with the result that as such a protrusion rotates to a location where the basal edges of two cells come together, the bleb causes a local displacement of the neighboring cell. If the blebbing be-

FIG. 6. (A) Morphology of the archenteron at the ½ gastrula stage. Basal surfaces are rounded. Bar = 10 μm. (B) Late in gastrulation, cells are elongated in the narrowest region of the archenteron (arrows). The elongated cells are aligned along the animal-vegetal axis. Bar = 10 μm.

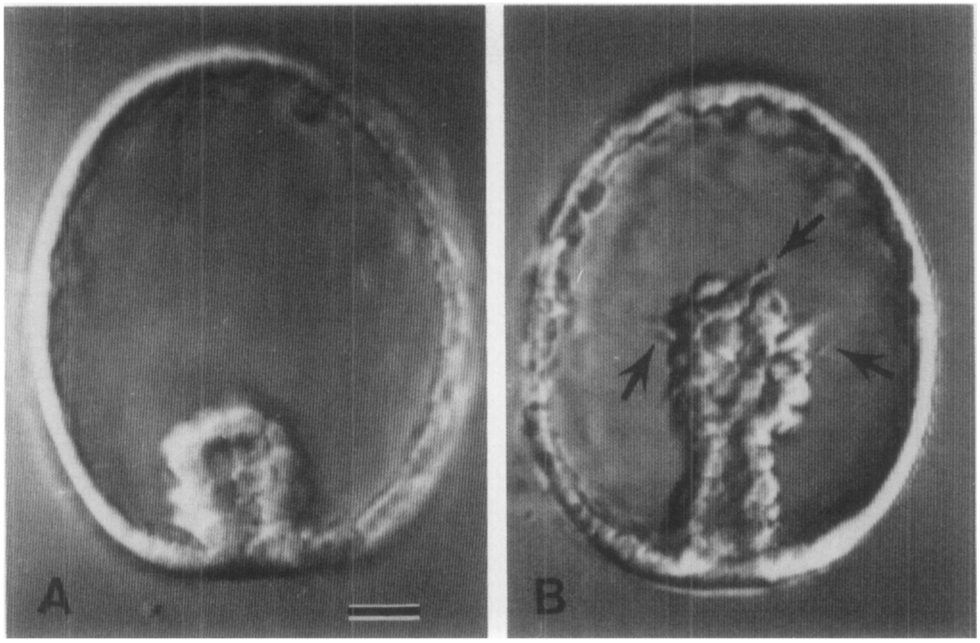

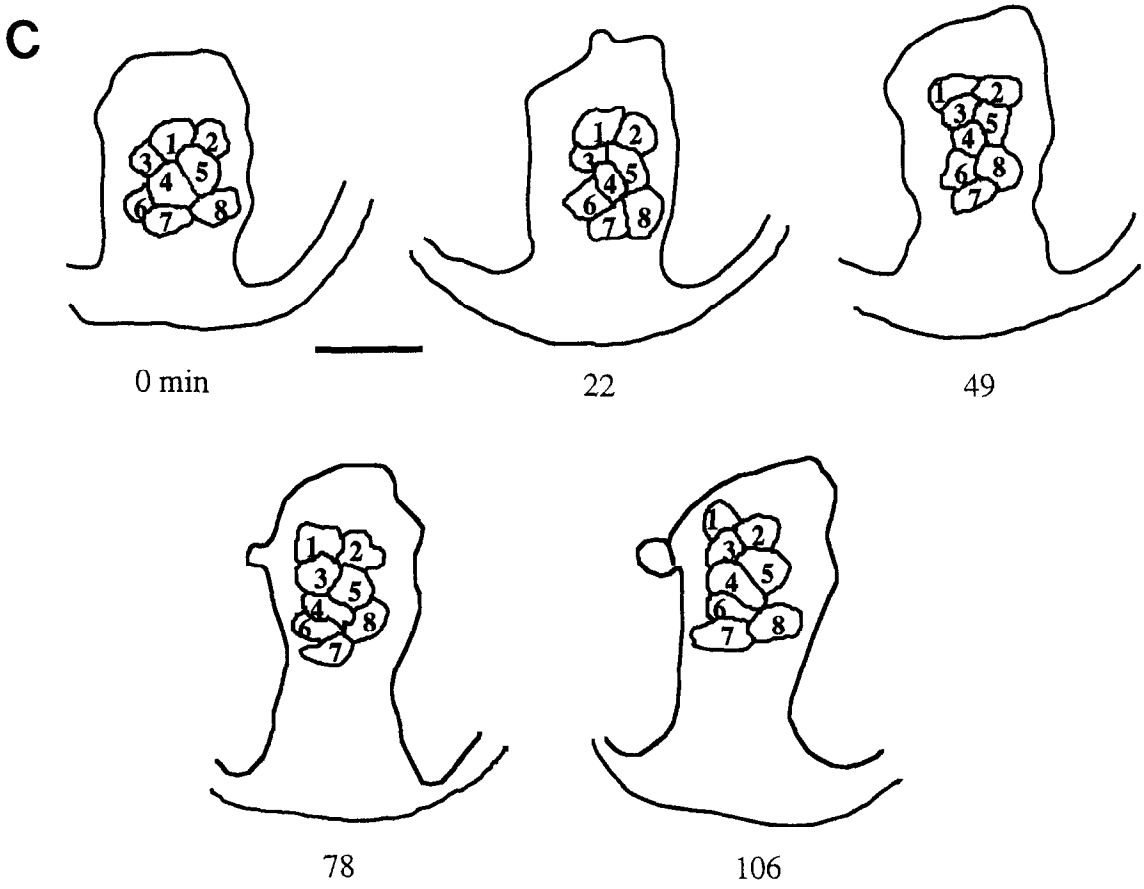

FIG. 8. Differential interference contrast micrographs of *Eucidaris* gastrulae photographed directly from the video monitor. (A) Early gastrula. Note the loose appearance and defined boundaries of the basal surfaces of cells in the archenteron. (B) Late gastrula. Filopodia still do not reach the animal pole (arrows). Bar = 25 μm. (C) Direct observation of cell rearrangement during gastrulation in *Eucidaris*. Tracings were made from the video monitor at the times indicated. Cells other than the array of cells numbered 1–8 have been omitted for clarity. Note that by the end of the period of observation, the array of cells narrows from three cells diameters in width to two, with a concomitant increase in length of the archenteron. Bar = 25 μm.

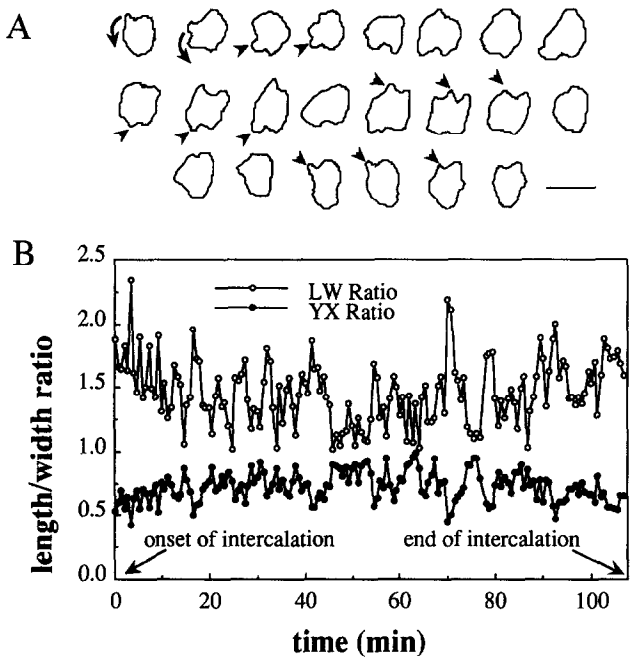

FIG. 9. Blebbing motility during cell rearrangement in *Eucidaris*. Tracings of an individual cell within the archenteron are shown at 20-sec intervals. Note the hemispherical blebs (arrows) that rotate around the basal periphery. Bar = 5 μm. (B) Temporal changes in cell shape during cell rearrangement in *Eucidaris*. Cell 6 from Fig. 8C was traced at 40-sec intervals, and its YX ratio was calculated and plotted over the duration of its intercalation between cells 4 and 7. The approximate time with respect to the intercalation event is also indicated (arrows).

havior of an individual cell known to be undergoing intercalation is followed, its basal surface can be seen to undergo fluctuations in its YX ratio over time (Fig. 9B). Thus the cell continually "squeezes" up and down and back and forth.

When these fluctuations in cell shape are examined using the tools of time series analysis (Box and Jenkins, 1976), it becomes apparent that they are not periodic. Figure 10A and B present the results of autocorrelation and partial autocorrelation analyses of the protrusive activity of the same cell described in Fig. 9B. The autocorrelation procedure involves shifting the data by a known phase, plotting the shifted data against the original data, and looking for phases that result in "constructive interference" that reflects periodicity. If the blebbing data are essentially a random walk, then no significant peaks will be seen at phase shifts greater than the "persistence" time of the average bleb (about 1 min). Fig. 10A shows that in fact no peaks of statistical significance occur for shifts of more than 1-2 min, i.e., the process is *not* periodic.

Partial autocorrelation analysis is a useful measure of the "memory" of a cell; significant correlations for various lag periods in this case reflect whether or not the state of the cell at a previous time point has a significant influence on what the cell is presently doing, after the subtraction of effects due to intervening time steps (for a similar type of analysis in the case of fibroblast motility, see Dunn and Brown, 1987). Fig. 10B shows that the state of the cell at any given time is only influenced by its state during the previous minute or so, i.e., *the cell has a short memory.* Indeed, the blebbing behavior can be accounted for completely by modeling it stochastically as an autoregressive moving average (ARMA) process, in which the state of a cell at time t is influenced by (1) its state over the past 1-2 min, but particularly its state during the immediately preceding time step, and (2) the "average" shape of the cell within a 1- to 2-min period centered on time t [i.e., an ARMA (2,1) process; the residuals are not significantly different from "white noise" for both YX ($P = 0.75$) and LW ratios ($P = 0.91$)]. This analysis is a rather tedious way of confirming the general impression one has from time-lapse footage: the archenteron is a collection of

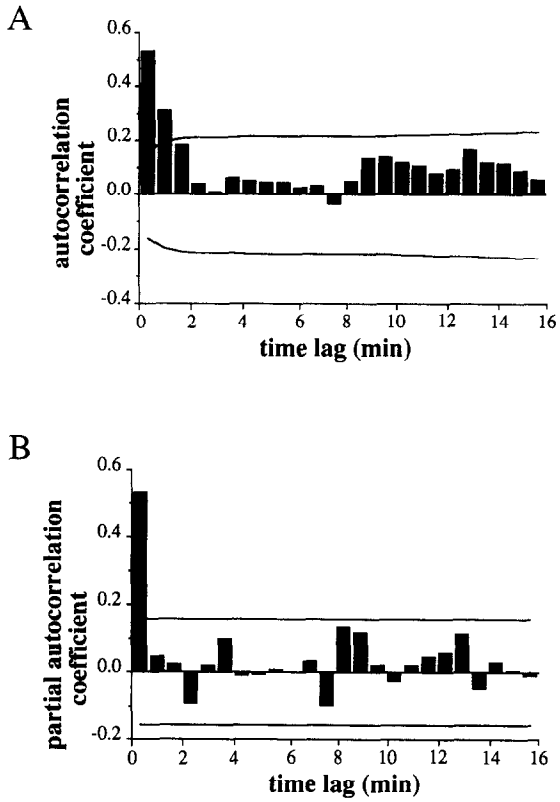

FIG. 10. Time series analysis of blebbing motility in *Eucidaris*. Autocorrelation plot of YX ratios for the cell analyzed in Fig. 9B for various lag times (min). Modeling the blebbing behavior as an ARMA(2,1) process results in no significant residual autocorrelations (see Results), and the following parameter values (see Box and Jenkins, 1976 for further details of the analysis procedures): AR(1) = 1.51 ± 0.15; AR(2) = −0.51 ± 0.15; MA(1) = 0.78 ± 0.10. (B) Partial autocorrelation plot of YX ratios for the same cell.

randomly active cells all performing, at the level of the current analysis, the same qualitative behavior. As a result, the overall impression one has is that the cells are "jostling" against one another continually as they rearrange. Ultimately, however, *successful* intercalation only occurs in the circumferential direction, with the result that the archenteron gradually narrows and lengthens.

DISCUSSION

Cells Are Not Added to the Archenteron as It Elongates

In *L. pictus,* cell division and DNA synthesis are unnecessary during secondary invagination (Stephens *et al.*, 1986). Moreover, the results of cell counts, vital dye marking, time-lapse videomicroscopy, and cellular volume measurements presented here indicate that few cells are normally added to the archenteron during secondary invagination in this species. Archenteron elongation in *L. pictus* appears to be a process intrinsic to those cells that have already invaginated during the first phase of gastrulation. This may not be the case in other species, however. For example, in *Lytechinus variegatus* regionalized cell division is extensive at the gastrula stage, and may contribute significantly to the process of invagination (Nislow and Morrill, 1988). Nevertheless, the results presented here indicate that cell division and involution *need not* occur to produce invagination of the archenteron.

Cell Rearrangement Occurs via Local Changes in Position

An impressive feature of morphogenetic movements mediated by cell rearrangement is that the concerted effect of many local, small shifts in cell position results in dramatic distortions of tissues (reviewed by Keller, 1987; Fristrom, 1988). The deformation of labeled chimaeric clones in *L. pictus* and direct observation of cell rearrangement in *Eucidaris* indicate that cells in the archenteron are only displaced with respect to one another by 1-2 cell diameters. When reproduced throughout the entire archenteron, these small shifts in position are sufficient to produce a 50-100% increase in its length. The situation is similar during *Drosophila* imaginal disc morphogenesis: although leg discs undergo extensive cell rearrangement during their eversion (Fristrom, 1976), mixing of cells at clonal boundaries within discs appears to involve a zone 1-2 cells wide, based on displacements of clonally related cells in genetic mosaics (Held, 1979). Near-neighbor analysis in *L. pictus* indicates that as the archenteron elongates to the $\frac{2}{3}$ gastrula stage, the cells of the archenteron depart most drastically from their original hexagonal packing. It is during this period that the *entire* archenteron experiences the greatest number of cell rearrangements. The residual departures from hexagonal packing remaining at the end of gastrulation probably reflect an inability of the epithelium to accommodate completely the cell rearrangements and shape changes that occur during secondary invagination and still retain a fully hexagonal arrangement.

Cells in the Archenteron Undergo Polarized Changes in Shape and Motility as They Rearrange

Cells flatten in the apical-basal direction. The cell flattening that occurs during archenteron elongation in *L. pictus* is extensive, and is tightly coupled to the cell rearrangement that occurs simultaneously. Flattening appears to occur to a greater or lesser extent in most, if not all, species of sea urchin (Dan and Inaba, 1968;), but here again the contribution probably varies depending on the species (for example, considerably less flattening occurs in *L. variegatus* than in *L. pictus*) (Morrill and Santos, 1985). Flattening is largely independent of filopodial traction, since it occurs in exogastrulae and after ablation of secondary mesenchyme cells in *L. pictus* (Hardin and Cheng, 1986; Hardin, 1988), and since the rate of flattening actually slows late in gastrulation, when filopodial activity is presumably most intense (present Results). Epithelial cell rearrangement is also accompanied by extensive flattening of the cells as they rearrange in other systems (*Drosophila* imaginal discs, Fristrom, 1976; the superficial layer of *Xenopus* gastrulae, Keller, 1978; teleost epiboly, Keller and Trinkaus, 1987). In all of these systems the processes of cell rearrangement and cell flattening must apparently work in tandem to dramatically change the linear dimensions of a tissue while simultaneously increasing its total surface area.

Cells are polarized along the axis of extension of the archenteron. The oriented lamellipodia that appear at the outset of secondary invagination demonstrate that all cells in the archenteron wall undergo a dramatic change in their program of motility when cell rearrangement begins. The orientation of the lamellipodia suggests that they are not directly involved in force production by contracting, since their contraction would result in shortening, rather than elongation, of the archenteron. Their transient appearance before cell rearrangement commences also makes it unlikely that they produce the forces for rearrangement. However, these protrusions do betray an inherent polarization of all cells in the archenteron along its axis of extension, which is presumably necessary for directed cell rearrangement (Keller and Hardin, 1987).

Cells are probably stretched due to filopodial tension.

The results of previous studies suggest that archenteron elongation in *L. pictus* involves two processes: (1) elongation by active cell rearrangement independent of filopodial traction by secondary mesenchyme cells, and (2) additional, filopodia-dependent cell rearrangement (Hardin and Cheng, 1986; Hardin, 1988). During the early stages of secondary invagination axial tension does not predominate within the archenteron, since the cells of the archenteron are not elongated prior to the $\frac{2}{3}$ gastrula stage. Filopodia-independent elongation is probably the dominant mechanism operating at this time. In contrast, previous studies using a number of different species have suggested that the effects of filopodial tension are most pronounced late in gastrulation (Okazaki, 1956; Gustafson and Kinnander, 1960; Hardin and Cheng, 1986). The results presented here support and extend these findings. The cells of the archenteron lengthen along the animal-vegetal axis at the $\frac{2}{3}$-$\frac{3}{4}$ gastrula stage, coinciding with a change in the orientation of the filopodia to a predominantly upward, or animal, direction (Hardin *et al.*, 1988). The reversion to a less elongated shape by the end of gastrulation further suggests that the archenteron responds to the concerted activity of the filopodia by additional cell rearrangement. That cells in the narrowest region of the archenteron in some embryos near the end of gastrulation are conspicuously elongated along the long axis of the archenteron suggests that in these embryos continued cell rearrangement is insufficient to completely relieve the tension generated by the filopodia. In contrast, such marked stretching is never observed in *Eucidaris*, probably because the overall distribution of the filopodia is lateral to the axis of extension, and hence there is no global, axial tension generated within the archenteron.

Cells Rearrange by Circumferential Intercalation

The time-lapse data presented here suggest that endoderm cells in *Eucidaris* employ *basal blebbing motility* during cell rearrangement. This apparently chaotic behavior is clearly capable of locally displacing neighboring cells, and is performed especially vigorously by cells undergoing intercalation. Although such behavior has only been conclusively demonstrated in intact embryos of *Eucidaris* thus far, there is some evidence that such blebbing motility is performed by euechinoid embryos as well. When *L. variegatus* gastrulae are dissociated, a subpopulation of the dissociated cells displays vigorous rotating blebs (McClay, 1986; J. Hardin and D. McClay, unpublished observations), and in incompletely dissociated embryos it is clear that at least many of these cells are endoderm cells (J. Hardin, unpublished observations). The rotating bleb-like motility appears similar to that envisioned by the "cortical tractor" model originally proposed by Jacobson *et al.* (1986) to account for cell rearrangement within the neural plate during urodele neurulation. These authors propose that such basal blebs could intercalate between cells at their basolateral margins and ultimately cause the rearrangement of cells via the upward (i.e., basal-to-apical) rotation of the protrusions (see also a modified version of this model proposed by Fristrom, 1988). The cells in the archenteron of *Eucidaris* display a prodigious capacity for motility of this sort, and if the success of intercalating protrusions is somehow biased in the circumferential direction, then such cortical motility may be a sufficient "motor" by which to drive cell rearrangement. Indeed one visible sign of such bias in *Eucidaris* as intercalation proceeds is the elongation of the cells perpendicular to the axis of extension, as they apparently wedge their way between one another (similar morphology is seen during development of the notochord and somitic mesoderm in chordates (Miyamoto and Crowther, 1985; Keller *et al.*, 1985; Thorogood and Wood, 1987; Wilson *et al.*, 1989)). One reason why such shape changes are not seen in *L. pictus* may be that filopodial tension tends to stretch the cells axially, thereby masking similar behavior in these embryos.

Such blebbing behavior may be an effective means for producing cell rearrangement, but how this general behavior is biased to produce intercalation is very much less clear. One suggested mechanism for producing directionality is adhesive disparities between the cells. For example, Jacobson *et al.* (1986) have suggested that cells in the amphibian neural plate rearrange to maximize their contact with the neural plate/epidermis boundary, with the result that elongation of the neural plate occurs along the anterior/posterior axis. Mittenthal and Mazo (1983) have suggested that adhesive disparities could account for the pattern of cell rearrangement seen during imaginal disc eversion in *Drosophila:* by minimizing the boundary between originally concentric zones of cells with adhesive disparities, they postulate that a flat disc will be converted into a cylinder with the originally concentric regions lying in a proximal-distal sequence along the everted disc. Late in sea urchin gastrulation the regions of the archenteron that will differentiate into the three compartments of the larval gut express spatially localized cell surface proteins (McClay *et al.*, 1983; Wessell and McClay, 1985; Coffman *et al.*, 1985), and if full archenteron elongation is prevented these markers are expressed in a compressed, concentric pattern (McClay *et al.*, 1989). Although these results imply that there are concentric zones of differentiation within the archenteron, it is not known what role if any these regional differences might play in gastrulation.

Cell Rearrangement Closes the Blastopore and Elongates the Archenteron Simultaneously

In *L. pictus* the blastopore decreases in diameter by ~35% during secondary invagination. Since this decrease is accompanied by cell rearrangement at the blastopore lip as well as at the base of the archenteron, it seems likely that these processes are coupled. It is not known whether the cells at the blastopore actively rearrange, or whether they rearrange to accommodate cellular movements within the archenteron. In either case, gastrulation in the sea urchin embryo bears a remarkable resemblance to amphibian gastrulation. In *Xenopus*, bottle cells constrict their apices dramatically to produce a shallow invagination at the blastopore lip (Hardin and Keller, 1988). Then the cells of the marginal zone rearrange via explosive blebbing motility (Keller and Hardin, 1987), resulting in dramatic deepening of the archenteron and simultaneous closure of the blastopore (Keller *et al.*, 1985; Keller and Danilchik, 1988). In the sea urchin embryo deepening of the archenteron also occurs via an initial invagination involving dramatic changes in cell shape followed by extensive cell rearrangement and concurrent blastopore closure. While there are significant differences between these two systems, the complex orchestration of gastrulation in these and other deuterostomes may involve a limited repertoire of basic morphogenetic movements (e.g., invagination and convergent cell rearrangement) which are shared in common across considerable phylogenetic distances.

I am deeply grateful to Nancy Benson of the Electron Microscope Laboratory, California State University, Hayward, for donating embedded embryos, and for initial help in preparing specimens for scanning electron microscopy. I also thank Greg Wray for instruction in the use of his chimaera technique and Chet Regen for timely technical assistance with digitizer hardware. The generous loan by Dr. Fred Nijhout of computer time to perform the time series analysis was invaluable. Discussions with Drs. Ray Keller, Fred Wilt, and Diane Fristrom were stimulating and helpful. The comments of Drs. Steve Black and Dave McClay on the manuscript were greatly appreciated. This work was supported by a NSF predoctoral fellowship, NIH Postdoctoral Fellowship GM122780, and a Duke University Hargitt Fellowship to the author, and by NIH Grants HD18979 to R. Keller, HD14503 to F. Wilt, and HD14483 to D. McClay.

REFERENCES

AMEMIYA, S., AKASAKA, K., and TERAYAMA, H. (1983). Scanning electron microscopy of gastrulation in a sea urchin (*Anthocidaris crassispina*). *J. Embryol. Exp. Morphol.* **67,** 27-35.

BOX, G. E. P., and JENKINS, G. M. (1976). "Time Series Analysis: Forecasting and Control," 2nd ed. Holden-Day, San Francisco.

CAMERON, R. A., HOUGH-EVANS, B. R., BRITTEN, R. J., and DAVIDSON, E. H. (1987). Lineage and fate of each blastomere of the eight-cell sea urchin embryo. *Genes Dev.* 1, 75-84.

COFFMAN, J., NELSON, S., and MCCLAY, D. R. (1985). A cell surface protein that identifies the ventral surface of the ectoderm of sea urchin gastrulae. *J. Cell Biol.* **101,** 469a.

DAN, K., and INABA, D. (1968). Echinoderma. *In* "Invertebrate Embryology" (M. Kumé and K. Dan, Eds.), pp. 280-332. NOLIT Pub., Belgrade.

DAN, K. and OKAZAKI, K. (1956). Cyto-embryological studies of sea urchins. III. Role of secondary mesenchyme cells in the formation of the primitive gut in sea urchin larvae. *Biol. Bull.* **110,** 29-42.

DUNN, G. A., and BROWN, A. F. (1987). A unified approach to analysing cell motility. *J. Cell Sci. (Suppl.)* **8,** 81-102.

ETTENSOHN, C. A. (1984a). Primary invagination of the vegetal plate during sea urchin gastrulation. *Amer. Zool.* **24,** 571-588.

ETTENSOHN, C. A. (1984b). "An Analysis of Invagination during Sea Urchin Gastrulation." Ph.D. dissertation, Yale University, New Haven, CT.

ETTENSOHN, C. A. (1985). Gastrulation in the sea urchin embryo is accompanied by the rearrangement of invaginating epithelial cells. *Dev. Biol.* **112,** 383-390.

FRISTROM, D. (1976). The mechanism of evagination of imaginal disks of Drosophila. III. Evidence for cell rearrangement. *Dev. Biol.* **54,** 163-171.

FRISTROM, D. (1988). The cellular basis of epithelial morphogenesis. A review. *Tissue Cell* **20,** 645-690.

GUSTAFSON, T., and KINNANDER, H. (1956). Microaquaria for time-lapse cinematographic studies of morphogenesis in swimming larvae and observations on gastrulation. *Exp. Cell Res.* **11,** 36-57.

GUSTAFSON, T., and KINNANDER, H. (1960). Cellular mechanisms in morphogenesis of the sea urchin gastrula. The oral contact. *Exp. Cell Res.* **21,** 361-373.

GUSTAFSON, T., and WOLPERT, L. (1967). Cellular movement and contact in sea urchin morphogenesis. *Biol. Rev.* **42,** 442-498.

HARDIN, J. D. (1986). Active epithelial cell rearrangement in the archenteron: A new mechanism for driving sea urchin gastrulation. *J. Cell Biol.* **103,** 3a.

HARDIN, J. D. (1987). Archenteron elongation in the sea urchin embryo is a microtubule-independent process. *Dev. Biol.* **121,** 253-262.

HARDIN, J. (1988). The role of secondary mesenchyme cells during sea urchin gastrulation studied by laser ablation. *Development* **103,** 317-324.

HARDIN, J. D., and CHENG, L. Y. (1986). The mechanisms and mechanics of archenteron elongation during sea urchin gastrulation. *Dev. Biol.* **115,** 490-501.

HARDIN, J., and KELLER, R. (1988). The behaviour and function of bottle of cells in gastrulation of *Xenopus laevis*. *Development* **103,** 211-230.

HARDIN, J., MORRILL, J., and MCCLAY, D. (1988). Mechanisms of filopodial guidance during sea urchin gastrulation. *J. Cell Biol.* **107,** 814a.

HELD, L. I. (1979). A high-resolution morphogenetic map of the second-leg basitarsus in *Drosophila melanogaster*. *Wilhelm Roux's Arch. Dev. Biol.* **187,** 129-150.

HOOK, G. R., and RASBAND, W. (1987). MacMeasure: A low-cost, easy-to-operate quantitative morphometrics system for the Macintosh computer. *In* "Proceedings of the 45th Annual Meeting of the Electron Microscopy Society of America" (G. W. Bailey, Ed.), pp. 920-921. San Francisco Press, San Francisco.

HÖRSTADIUS, S. (1935). Über die Determination im Verlaufe der Eiachse bei Seeigeln. *Pubbl. Staz. Zool. Napoli* **14,** 251-429.

HÖRSTADIUS, S. (1973). "Experimental Embryology of Echinoderms." Clarendon Press, Oxford.

JACOBSON, A. G., OSTER, G. F., ODELL, G. M., and CHENG, L. Y. (1986). Neurulation and the cortical tractor model for epithelial folding. *J. Embryol. Exp. Morphol.* **96,** 19-49.

KELLER, R. E. (1978). Time-lapse cinematographic analysis of super-

ficial cell behavior during and prior to gastrulation in *Xenopus laevis*. *J. Morphol.* **157,** 223–248.

KELLER, R. E. (1987). Cell rearrangement in morphogenesis. *Zool. Sci.* **4,** 763–779.

KELLER, R., and DANILCHIK, M. (1988). Regional expression, pattern and timing of convergence and extension during gastrulation of *Xenopus laevis*. *Development* **103,** 193–210.

KELLER, R. E., DANILCHIK, M., GIMLICH, R., and SHIH, J. (1985). The function and mechanism of convergent extension during gastrulation of *Xenopus laevis*. *J. Embryol. Exp. Morphol.* (*Suppl.*) **89,** 185–209.

KELLER, R., and HARDIN, J. (1987). Cell behavior during active cell rearrangement: Evidence and speculations. *J. Cell Sci.* (*Suppl.*) **8,** 369–393.

KELLER, R., and TRINKAUS, J. (1987). Rearrangement of enveloping layer cells without disruption of the epithelial permeability barrier as a factor in *Fundulus* epiboly. *Dev. Biol.* **120,** 12–24.

KINNANDER, H., and GUSTAFSON, T. (1960). Further studies on the cellular basis of gastrulation in the sea urchin larva. *Exp. Cell Res.* **19,** 276–290.

MCCLAY, D. R. (1986). Embryo dissociation, cell isolation, and cell reassociation. *Methods Cell Biol.* **27,** 309–323.

MCCLAY, D., ALLIEGRO, M. C., and HARDIN, J. D. (1989). Cell interactions as epigenetic signals in morphogenesis of the sea urchin embryo. *In* "The Cellular and Molecular Biology of Pattern Formation" (D. Stocum Ed.). Oxford, Oxford University Press. (In press)

MCCLAY, D. R., CANNON, G. W., WESSELL, G. M., FINK, R. D., and MARCHASE, R. B. (1983). Patterns of antigenic expression in early sea urchin development. *In* "Time, Space, and Pattern in Embryonic Development" (W. Jeffery and R. Raff, Eds.), pp. 157–169. A. R. Liss, New York.

MITTENTHAL, J. and MAZO, R. (1983). A model for shape generation by strain and cell-cell adhesion in the epithelium of an arthropod leg segment. *J. Theor. Biol.* **100,** 443–483.

MIYAMOTO, D., and CROWTHER, R. (1985). Formation of the notochord in living ascidian embryos. *J. Embryol. Exp. Morphol.* **86,** 1–17.

MORRILL, J. B., and SANTOS, L. L. (1985). A scanning electron microscopical overview of cellular and extracellular patterns during blastulation and gastrulation in the sea urchin, *Lytechinus variegatus*. *In* "The Cellular and Molecular Biology of Invertebrate Development" (R. H. Sawyer and R. M. Showman, Eds.), pp. 3–33. University South Carolina Press, Columbia, SC.

NISLOW, C., and MORRILL, J. B. (1988). Regionalized cell division during sea urchin gastrulation contributes to archenteron formation and is correlated with the establishment of larval symmetry. *Develop. Growth Differ.* **30,** 483–499.

OKAZAKI, K. (1956). Exogastrulation induced by calcium deficiency in the sea urchin, *Pseudocentrotus depressus*. *Embryologia* **3,** 23–36.

OKAZAKI, K. (1975). Normal development to metamorphosis. *In* "The Sea Urchin Embryo" (G. Czihak, Ed.), pp. 177–232. Springer-Verlag, Berlin.

SCHROEDER, T. (1981). Development of a "primitive" sea urchin (*Eucidaris tribuloides*): Irregularities in the hyaline layer, micromeres, and primary mesenchyme. *Biol. Bull.* **161,** 141–151.

SOKAL, R. R., and ROHLF, F. J. (1981). "Biometry," 2nd ed. Freeman, New York.

STEPHENS, L., HARDIN, J., KELLER, R., and WILT, F. (1986). The effects of aphidicolin on morphogenesis and differentiation in the sea urchin embryo. *Dev. Biol.* **118,** 64–69.

THOROGOOD, P., and WOOD, A. (1987). Analysis of *in vivo* cell movement using transparent tissue systems. *J. Cell Sci.* (*Suppl.*) **8,** 395–413.

WESSELL, G. M., and MCCLAY, D. R. (1985). Sequential expression of germ-layer specific molecules in the sea urchin embryo. *Dev. Biol.* **111,** 451–463.

WILSON, P. A., OSTER, G., and KELLER, R. (1989). Cell rearrangement and segmentation in *Xenopus:* Direct observation of cultured explants. *Development* **105,** 155–166.

WRAY, G. A. (1987). "Heterochrony and Homology in the Evolution of Echinoid Development." Ph.D. dissertation, Duke University, Durham, NC.

WRAY, G. A., and MCCLAY, D. R. (1988). The origin of spicule-forming cells in a primitive sea urchin that appears to lack primary mesenchyme. *Development* **103,** 307–316.

ZAR, J. H. (1984). "Biostatistical Analysis," 2nd ed. Prentice-Hall, Englewood Cliffs, NJ.